Universality of extreme broadening mechanisms in some near-edge x-ray spectra

Terrence Jach,[1,*] John Vinson,[1] Michael A. Woodcox,[1] Adrian Jonas,[2]
Katja Frenzel,[2] Rainer Unterumsberger,[2,†] and Burkhard Beckhoff[2]

[1] *Material Measurement Laboratory, National Institute of Standards and Technology, Gaithersburg, MD 20899*
[2] *Physikalisch-Technische Bundesanstalt, Abbestraße 2-12, 10587 Berlin, Germany*

(Dated: December 30, 2024)

Extreme broadening previously observed in certain N x-ray fluorescence lines excited near the N K-edge in nitrates has been observed in the S L x-ray fluorescence in sodium sulfate, Na_2SO_4. It is explained as a large imaginary self-energy corresponding to an anomalously short lifetime of quasiparticles in one of the valence bands of these compounds. Our latest measurement and the corresponding many-body theory indicate that this is a general effect not specific to nitrates.

I. INTRODUCTION

Previously reported soft x-ray spectra from nitrogen compounds have demonstrated that one of the expected N fluorescence lines had "disappeared", or at least, was not obviously present [1]. Subsequent observations of x-ray fluorescence near the N K-edge of NH_4NO_3 confirmed that the line was observable but spread out over a width of 4 eV [2]. Theoretical calculations of the band theory, once they included first-order many-body corrections, provided a mechanism by which this could be understood [3].

The effect has since been confirmed in N K fluorescence near the K edge in other nitrate compounds [4]. The N K x-ray fluorescence line that is observed at the lowest energy shows a broadening that is totally inconsistent with the other features. It corresponds to a 1s hole that is filled from p-projected states in the lowest lying valence band. The band in the crystal derives from the N-O σ bond in the NO_3^- ion.

Theory supplies an explanation for this effect in a straightforward manner. A purely density-functional theory (DFT) calculation predicts that in nitrates this band should have little dispersion and almost no width in energy — a quasimolecular state. When this is corrected for many-body effects by means of a GW calculation [5], the situation changes drastically. In addition to a significant energy correction to all the bands due to the real part of the self-energy, the imaginary part of the self-energy is nonzero for the lowest bands. This means that, unlike normal quasiparticles that have effectively an infinite lifetime, the quasiparticles in the lowest bands have short lifetimes and undergo rapid fluctuations.

A logical next step is to determine whether this is a peculiarity of the nitrate bonding and band structure of a specific crystal symmetry or a more general effect. We have investigated the S x-ray fluorescence in sodium sulfate, Na_2SO_4, near the S $L_{2,3}$-edge, both experimentally and theoretically. This compound is a particularly good test of the effect, since the band gap, nearly 9 eV, is greater than that of the previous compounds that we have studied, and there are bands extending fully down to 25 eV below the top of the valence band. We confirm that a similar effect is strongly observed in the lowest lying x-ray fluorescence line corresponding to a 2p hole filled from the valence bands originating from the S-O σ bond. The band structure of Na_2SO_4 is significantly different from that of the nitrates. It appears that the anomalous broadening effect that we observe is of a more general nature rather than a unique case

In our previous studies we investigated ammonium nitrate, which forms an orthorhombic structure of symmetry Pmmm [2, 3], and lithium nitrate, which forms a trigonal structure of symmetry $R\bar{3}c$ [4]. In contrast, anhydrous sodium sulfate, Na_2SO_4, crystalizes as an orthorhombic crystal with the Fddd summetry [6]. The samples therefore represent different crystal symmetries. While the nitrate ion in the crystals is planar, the sulfate group is tetrahedral.

A. Lifetime broadening within the GW approximation

Despite strong interactions between electrons, excitations away from the ground state can often be treated within the quasiparticle approximation. The truly single-particle excitations of the non-interacting system have corresponding quasiparticle excitations in the presence of interactions. Within many-body perturbation theory, the GW approximation provides a prescription for dressing the non-interacting single-particles to give the quasiparticles [5]. In this approximation the dynamic self-energy is given by $\Sigma(E) = iGW$, where G is the one-particle Green's function and W is the screened Coulomb interaction. The self-energy is complex-valued, and within the quasiparticle approximation this can be seen as providing an energy shift from the non-interacting to interacting system as well as a lifetime of the quasiparticle (from the inverse of the lifetime). This GW lifetime is not the only source of lifetime broadening as it included only electron terms, neglecting electron-phonon

* terrence.jach@nist.gov
† Present address: Helmut Fischer GmbH Institut für Elektronik und Messtechnik, Industriestraße 21, 71069 Sindelfingen, Germany

scattering or radiative decay. It also neglects phonon dynamics, where electronic excitations may cause ionic motion, changing the total state, e.g., in an extreme case photo-disassociation.

Later we will evaluate the GW self-energy corrections for Na_2SO_4 numerically, but here we will highlight under what conditions a large magnitude imaginary component could arise. The self-energy can be separated into a static, real-valued exchange and a dynamic, complex correlation part. As our interest is in the imaginary part of the self-energy we will restrict our discussion here to the correlation part Σ^c, which is given by separating the screened Coulomb into $W^c = W - v$. Similar arguments are laid out in Ref. [**?**]. Within the random-phase approximation the dielectric screening is given by non-interacting electron-hole excitations, and can be written as

$$W^c(\mathbf{r},\mathbf{r}',\omega) = \sum_s V^s(\mathbf{r})V^s(\mathbf{r}')\times \times\left(\frac{1}{\omega-\omega_s+i\eta}+\frac{1}{\omega+\omega_s-i\eta}\right) \quad (1)$$

where V^s are the fluctuation potentials arising from the density ρ of a single electron-hole (neutral) excitation

$$V^s(\mathbf{r}) = \int d^3r' \frac{\rho(r')}{|\mathbf{r}-\mathbf{r}'|} \quad (2)$$

with energies ω_s given by the single particle excitation energy difference. The Green's function can be written as a sum over states, and for periodic boundary conditions this can be done as a sum over all bands n and crystal momentum q,

$$G(\mathbf{r},\mathbf{r}',\omega) = \sum_{n\mathbf{q}} \frac{\psi_{n\mathbf{q}}(\mathbf{r})\psi^*_{n,\mathbf{q}}(\mathbf{r}')}{\omega - E_{n,\mathbf{q}} + i\eta\mathrm{sgn}(E_{nq}-E_F)} \quad (3)$$

where the sign of η depends on if the state is above or below the Fermi level E_F. We can then express the correlation part of the self energy

$$\Sigma^c(\mathbf{r},\mathbf{r}',E) = \frac{i}{2\pi}\int d\omega e^{-i\omega\eta}\sum_{n,\mathbf{q},s}\frac{V^s(\mathbf{r})V^s(\mathbf{r}')\psi_{n\mathbf{q}}(\mathbf{r})\psi^*_{n,\mathbf{q}}(\mathbf{r}')}{E-\omega-E_{n,\mathbf{k}+\mathbf{q}}+i\eta\mathrm{sgn}(E_{nq}-E_F)}\left(\frac{1}{\omega-\omega_s+i\eta}+\frac{1}{\omega+\omega_s-i\eta}\right) \quad (4)$$

Echoing Ref. [**?**], we carry out the integral over ω, and the imaginary part of Σ^c is given by

$$\mathrm{Im}\Sigma^c(\mathbf{r},\mathbf{r}',E) = \sum_{n,\mathbf{q},s} V^s(\mathbf{r})V^s(\mathbf{r}')\psi_{n\mathbf{q}}(\mathbf{r})\psi^*_{n,\mathbf{q}}(\mathbf{r}') \times \pi\delta(E\pm\omega_s - E_{n,\mathbf{k}+\mathbf{q}}) \quad (5)$$

where + (−) is for when $E_{n,\mathbf{k}+\mathbf{q}}$ is below (above) the Fermi level. The energies of the particle-hole fluctuations that make up the screening ω_s are strictly positive and equal or greater than the band gap. Looking at Eq. 5, the self-energy for an occupied state or quasihole ($E < E_F$) only has contributions from other occupied states that are higher in energy (closer to the top of the valence) by at least the band gap energy. Conceptually, for a filled Fermi sea at T≈0 with a single hole, only states higher in energy can scatter into it, and then only if they can conserve energy by creating a secondary excitation.

Short of evaluating the expressions numerically, we can estimate when GW lifetimes might be significant. A matrix element for a given state $\mathrm{Im}\langle m\mathbf{k}|\Sigma^c(E)|m\mathbf{k}\rangle$ involves an overlap with both the fluctuation potentials and intermediate states $n,\mathbf{q}$. This means for state m to have a large broadening there need to be upper valence bands n with a spatial overlap with m and that the dielectric response of the material for energies $|E_m - E_n|$ be spatially colocated as well. As we will see, these conditions are not met for the Na 2p orbitals as the upper valences bands are concentrated around the SO_4^{2-} ions, and despite being deep in the valence, the Na 2p has almost no GW broadening. Similarly, deep core levels have no shortage of higher-energy valence orbitals to couple to, but their overlap is weaker as is the dielectric response.

II. COMPUTATIONAL DETAILS

Calculations of the X-ray absorption and emission are carried out using the Bethe-Salpeter equation (BSE) formalism as implemented in the OCEAN code [7, 8]. We will review the BSE approach as implemented in OCEAN here only briefly, and refer the reader to Ref. 8 for more details. The x-ray absorption spectrum can be written as proportional to the imaginary part of the dielectric response

$$\sigma(\omega) \propto \langle\Phi_0|T^\dagger_{\mathbf{q},\hat{\epsilon}}G_{\mathrm{BSE}}(\omega,\mathbf{q})T_{\mathbf{q},\hat{\epsilon}}|\Phi_0\rangle \quad (6)$$

where Φ_0 is the ground-state of the system and the operator T is the interaction between an electron and a photon of momentum $\mathbf{q}$ and polarization $\hat{\epsilon}$. The BSE

Green's function is an electron-hole propagator given by

$$G_{\mathrm{BSE}}(\omega) = \left[\omega - H_0^{(e)} + H_0^{(h)} + W - V_X\right]^{-1} \quad (7)$$

where $H_0^{(e,h)}$ are the single-particle Hamiltonians for the electron and hole, and the two electron-hole interaction terms are given by the attractive direct (W) and the repulsive exchange (V_X).

Here, the ground state Φ_0 is constructed from the occupied orbitals from the DFT calculation. The single-particle Green's functions also use DFT orbitals and eigenenergies corrected with a many-body self-energy correction (see Sec. II B below). The ions are considered to be fixed during the x-ray excitation process, and so Eq. 7 has no explicit reference to atomic coordinates. This is equivalent to the statement that the vibrational excitations in the system have small energies compared to the lifetime broadening, and the result is that the spectra reflect the initial-state atomic positions. However, even in a defect-free sample, the ions are vibrating around their equilibrium positions and this initial-state disorder is known to cause changes in the x-ray spectra [2].

A. Molecular dynamics

To model the initial state disorder, driven by vibrations, we carried out *ab initio* molecular dynamics calculations using the Vienna *Ab initio* Simulation Package (VASP) [9–11]. VASP uses a plane wave basis set, and ion-electron interactions were approximated using the projector-augmented wave (PAW) potentials [12]. A plane wave energy cutoff of 500 eV and a Γ-centered 5×5×5 Monkhorst-Pack [13] k-point grid were used for all calculations. Gaussian smearing was used for sampling of the Brillouin zone. The Perdew-Burke-Ernzerhof (PBE) functional [14] was used for all calculations, with the inclusion of van der Waals (vdW) interactions by means of the Grimme zero-damping method (DFT-D3) [15].

A 2×2×2 supercell of Na_2SO_4 was used to reduce interactions between the atoms and their images across the periodic boundary. All simulations were run using the canonical ensemble (NVT) at room temperature (298 K), with a 1 fs time step. Equilibration of the internal pressure and atomic positions was performed for 10 ps, followed by a 25 ps production run. Atomic positions were sampled every 2.5 ps providing a total of 10 snapshots for x-ray calculations.

B. Self-energy corrections

GW self-energy corrections to the DFT energies were calculated for the Na_2SO_4 unit cell using the ABINIT code [16, 17]. We used the Perdew-Burke-Ernzerhof (PBE) exchange-correlation potential [14], and pseudopotentials were taken from the PseudoDojo collection [18] and generated using ONCVPSP [19]. A planewave cutoff energy of 91 Ry was used, and the atomic positions were adjusted until the forces on each atom were less than 5×10^{-5} Ryd a.u.$^{-1}$. A $4 \times 4 \times 4$ Γ-centered k-point grid was used, yielding 18 inequivalent points in the Brillouin zone. A 16 Ryd cut-off was used for the dielectric matrix and 560 total bands were included. The dielectric response was calculated for frequencies from 0 eV to 24 eV at a spacing of 0.5 eV. *GW* corrections were calculated for the valence bands and 64 lowest conduction bands. We note that the correction for the Na $2s$ semi-core states is not converged, but these states are not detectable in our experiment and play no role in our analysis.

Using Wannier interpolation with the aid of the Wannier90 code, we show the interpolated band structure for the occupied states in Fig. 1 [20]. The bands are colored based on the imaginary part of their self-energy corrections, or, equivalently, their lifetime broadening due to electron-electron scattering. For reference, the S 2p core holes have a lifetime broadening of about 0.09 eV [21]. The upper valence bands, above −7 eV, show almost no lifetime broadening, $\lessapprox 0.01$ eV. The pair of bands around −8 eV has a small 0.04 eV broadening. Interestingly, the broadening of these bands has been shown experimentally to have a strong cation dependance in SO_4^{2-} compounds [22]. Substantially larger broadening is found for the six SOσ bands around −20 eV (1.2 eV to 1.5 eV) and for the two S $3s$ orbitals around −23 eV (0.6 eV). The Na $3p$ states at −25 eV are much more core-like. They do not couple strongly with transitions to the other valence bands and have a relatively small 0.02 eV broadening.

Our calculations indicate that at the PBE or PBE+G^0W^0 level the ordered unit cell of Na_2SO_4 has an indirect gap. While the conduction band minimum is at the Γ point, the valence band maximum at Γ is approximately 0.03 eV below its true maximum along the line between Γ and X. The fundamental gap within PBE is 5.37 eV, while the G^0W^0 corrections increase this to 8.40 eV, for a correction of 3.04 eV. The disordered supercells have an average PBE band gap of 5.18±0.12 eV, implying that the electron-phonon coupling reduces the gap by approximately 0.2 eV. Assuming that the *GW* correction is independent of the vibrational disorder, this gives a final calculated band gap of 8.2±0.1 eV. However, the relative alignment of the x-ray emission and absorption spectra requires an additional 2 eV gap correction, yielding a total of 10.2 eV.

C. X-ray calculations

X-ray spectra were calculated using the OCEAN code [7, 8]. Input DFT orbitals were calculated using the QUANTUM ESPRESSO code [23, 24] with the same pseudopotentials as for the earlier self-energy calculations and PBE exchange-correlation functional. Each $2 \times 2 \times 2$ supercell of Na_2SO_4 from the molecular dynamics calcu-

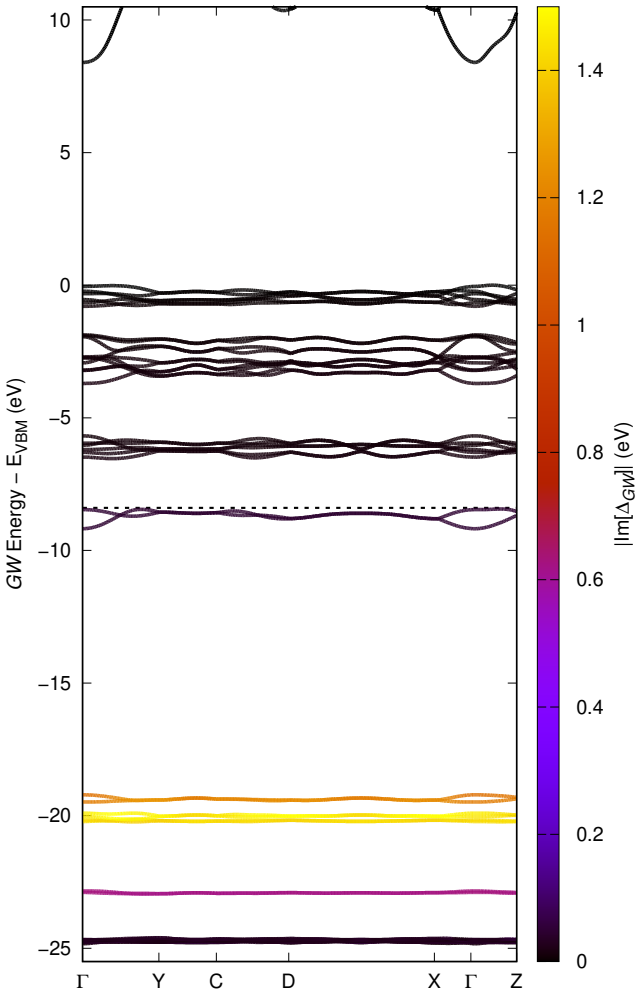

FIG. 1. Band structure of Na_2SO_4 determined from DFT calculations with G^0W^0 corrections. The bands are colored based on the complex value of their GW correction. The dashed line is the energy below the top of the valence band corresponding to the value of the calculated band gap. The bottom of the conduction band is included, showing the conduction band minimum at Γ.

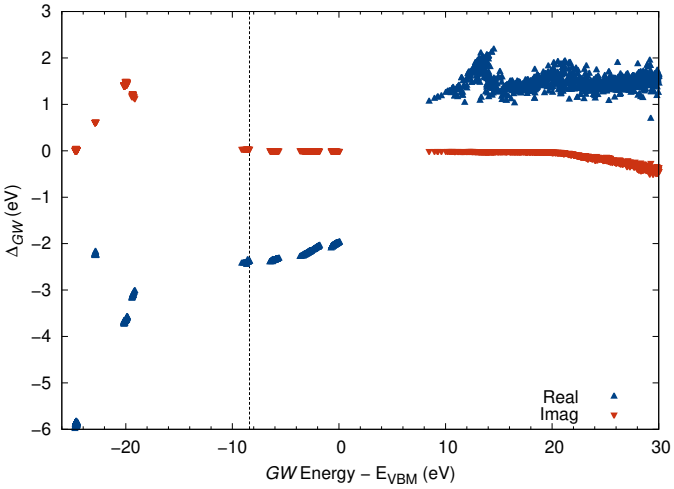

FIG. 2. The real (dark, blue) and imaginary (light, red) components of the G^0W^0 corrections of Na_2SO_4 as a function of the calculated G^0W^0 energy, with the valence band maximum set to 0 eV. Note, by convention the imaginary component is positive for occupied states and negative for unoccupied. The dashed line is the energy below the top of the valence band corresponding to the value of the calculated band gap.

lation has a total of 112 atoms with 16 S sites. A 2^3 k-point sampling and 886 conduction bands were used for the BSE final states. A 2^3 k-point sampling and 4000 bands were used for the screening calculation. The S $L_{2,3}$-edge absorption and emission spectra are calculated for each snapshot by summing over contributions from every S atom. Note that, for resonant inelastic soft x-ray scattering (RIXS), this summation is done coherently. We calculate the variance in the mean to give the statistical uncertainty in only averaging over 10 snapshots and show it as a shaded region in the plots of the calculated spectra showing the 95% confidence interval.

Prior to solving the BSE, both valence and conduction band energies underwent band-averaged GW energy corrections, based on the unit cell GW calculation detailed above. For each band, the average GW correction is calculated based on a weighted sum of the 18 symmetry-unique k-points. For the supercell calculations, the same correction is applied to groups of 8 bands, *e.g.*, the correction calculated for band 48 of the unit cell, the highest valence band, is applied to bands 377 through 384 of the supercells. The imaginary part of the correction to the conduction band states is negligible until about 12 eV above the conduction band minimum and then increases slowly in magnitude (see Fig. 2). For the x-ray absorption calculations only the real part of the GW corrections are included, and the resulting spectra are further broadened by Lorentzian of 0.09 eV full-width at half-maximum (FWHM) to match the expected core hole lifetime and a 0.28 eV FWHM Gaussian instrument resolution. For the emission spectra, we apply the same broadening as for the XAS, but also include the calculated imaginary GW broadening by separating the spectra by energy.

III. EXPERIMENTAL DETAILS

The experiments were carried out on the PTB U49 undulator beamline operated by the Physikalisch-Technische Bundesanstalt at the BESSY II synchrotron radiation source. The beamline and its plane grating monochromator have been described previously [25]. The sample was a pressed powder of anhydrous Na_2SO_4, and the spectra were obtained at room temperature in ultra-high vacuum. Near-edge x-ray absorption spectra were obtained both from characteristic S L-fluorescence monitored by a calibrated windowless silicon drift detector (SDD) at an angle of 45° out of the scattering plane

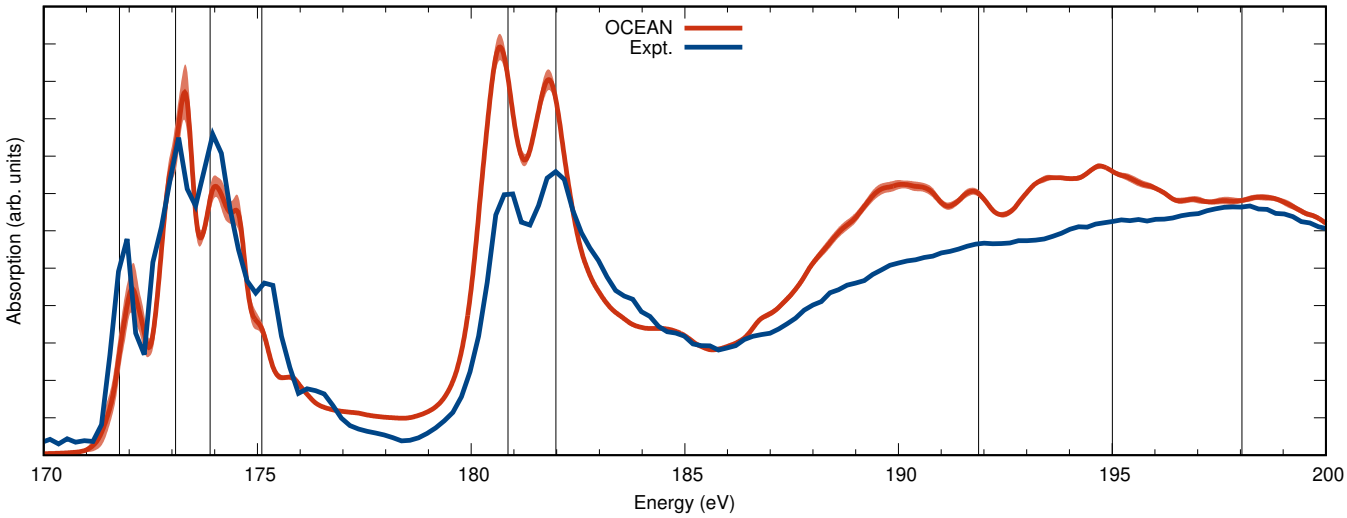

FIG. 3. X-ray absorption spectrum of Na_2SO_4 (dark, blue) at the S $L_{2,3}$-edge with the calculated *GW*-BSE spectrum (light, red). Vertical lines denote the incident x-ray energies of the RIXS. The width of the theory curve shows the statistical uncertainty in the mean (see text).

and from the sample current, both normalized to the beam intensity. The monochromator was calibrated in the vicinity of the S $L_{2,3}$-edge using x-ray absorption spectra from SF_6 in a gas cell detected by a diode. In this case, the molecular absorption lines were fitted over an energy range 170 eV-200 eV to a standard series of energies [26]. The energy uncertainty to one standard deviation was 0.053 eV.

X-ray emission spectra were originally obtained with a spherical grating on a Rowland Circle with a charge-coupled device (CCD) detector that has been previously described [27]. A 300 line/mm grating was used in first order. The x-ray spectrometer was horizontally mounted at 90° from the direction of the monochromator beam, which is incident onto the sample at 45°. The horizontal polarization of the undulator beam was therefore p-polarized. The energy range covered by the CCD was 142 eV-170 eV. Quasi-elastic scattering by a MoS_2 target from the energy-calibrated monochromator beam was employed to calibrate the energy scale of the spectrometer at 1 eV intervals over the range 160 eV-170 eV. The energy range was linear to within a standard deviation of 0.027 eV over this energy range.

Further spectra were obtained when the spectrometer was replaced with a spherical mirror/variable line-spacing (VLS) grating spectrometer of the Hettrick and Underwood design [28]. The average line spacing of the grating was 600 line/mm. The new spectrometer covered a range of 120-200 eV on a CCD. The increased energy range allowed us to observe the entire x-ray emission from Na_2SO_4 in a single spectrum. The optical geometry and the performance of the spectrometer will be described elsewhere. However, the solid angle collection efficiency of the spectrometer was improved over that of the spherical grating spectrometer by more than one order of magnitude, and the resolution over the enhanced energy range was improved by approximately a factor of 2. At each excitation energy, emission spectra were collected from an illuminated spot on the sample of 100 μm diameter for a total of 7440 s. The sample was displaced by one diameter every 120 s to minimize radiation damage.

This type of spectrometer produces spectra with a non-linear energy scale. In order to obtain accurate energies for the spectral features, it was necessary to record quasielastic (Rayleigh) scattering peaks that covered the entire range of the spectrum. Because of the increased solid angle collection efficiency, it was possible to cover this range with quasielastic scattering from the Na_2SO_4 sample itself, including below the S $L_{2,3}$-edge. Quasielastic peaks over the energy range 130 eV-198 eV were then fitted with Gaussian/Lorentzian lineshapes to a 4th order polynomial with a standard deviation of 0.012 eV over the entire energy scale. The spectrometer resolution, including the width of the monochromator radiation, as determined by fitting the linewidth of quasielastic scattering from MoS_2 was 0.28 eV. The independently calibrated spectra obtained with the spherical grating spectrometer and the VLS spectrometer were then observed to align precisely over their common energy range. The RIXS presented here are the data from the VLS spectrometer.

IV. X-RAY SPECTRA

A. X-ray absorption

An x-ray absorption spectrum taken in the vicinity of the S $L_{2,3}$-edge of Na_2SO_4 is shown in Fig. 3. A compar-

ison with the theoretical calculation for single electron excitation is shown. The doublet features are due to the splitting between the S $2p_{3/2}$ and $2p_{1/2}$ levels of 1.2 eV. The vertical lines indicate excitation energies at which details occur in the absorption spectrum. X-ray emission spectra were obtained for those energies.

B. RIXS

X-ray emission spectra are shown in Fig. 4 for the selected energies marked in the absorption spectrum of Fig. 3. The corresponding theoretical calculated spectra are shown. The correction for many-body effects using the *GW* approximation has been applied to the theory. Each theoretical spectrum shown was then averaged over multiple snapshots, averaging over disorder to the lattice outlined in Section II A. A single calculated spectrum without the *GW* correction is also displayed in the highest lying excitation energy of 198.0 eV in order to illustrate the consequences of the many-body effects.

The spectra change rapidly in the immediate vicinity of the S $L_{2,3}$-edge, due to the screening of the core hole due to the presence of the exciton. Two-body calculations in the Bethe-Salpeter equation account reasonably well for the rapid changes in the first 8 eV. We attribute the gradual shift of the main emission features upward in the excitation energy range between threshold and 175 eV to the final state conduction-electron–valence-hole excitonic binding, which becomes weaker as the excited electron goes into more diffuse, higher energy states. Features observed in the region 148 eV-152 eV do not occur in the theory. The feature observed around 152 eV has been previously identified as originating from the presence of Na_2SO_3, which may be present as a result of radiation damage [22].

Below 147 eV, the emission lines are extraordinarily broadened. This can be explained within the quasiparticle approximation, where, consistent with the *GW* and BSE approximations, the x-ray excitations of the system are treated as the creation of a quasi-electron and a quasi-hole. These quasi-particles are dressed by interactions with the rest of the system, and, importantly, they can decay. Quasiparticles have complex energies, where the imaginary part is proportional to the inverse of their lifetime. This approximation is inherent in the description of core-hole lifetime broadening, e.g., the 0.09 eV broadening of the S 2p holes. Our calculation of the *GW* self-energy (see Figs. 1 and 2) shows that the valence-band states contributing to emission below 147 eV have large lifetime broadenings.

The physical explanation is that the hole in the valence band (created when filling the core hole) is a quasiparticle that can decay by scattering into other valence band states. The quasihole's energy (and momentum) loss from this decay must be conserved, such as through the creation of an electron-hole excitation, e.g., an Auger-like process. In a metal, such excitations can be created down to nearly zero energy. In the case of an insulating compound such as we are studying here, electron-hole excitations must have an energy sufficient to span the band gap. Therefore, quasiholes in the upper valence bands cannot decay via electron-hole excitations. They decay via slower methods such as phonon scattering or even radiative scattering and have relatively long lifetimes. Deeper in the valence band, specifically at an energy of more than the band gap below the valence band maximum, quasiholes are able to decay via electron-hole excitations, resulting in very short lifetimes. The short lifetimes of these quasiparticles contribute to a final state that is unusually broad, a detail that is manifest as a large

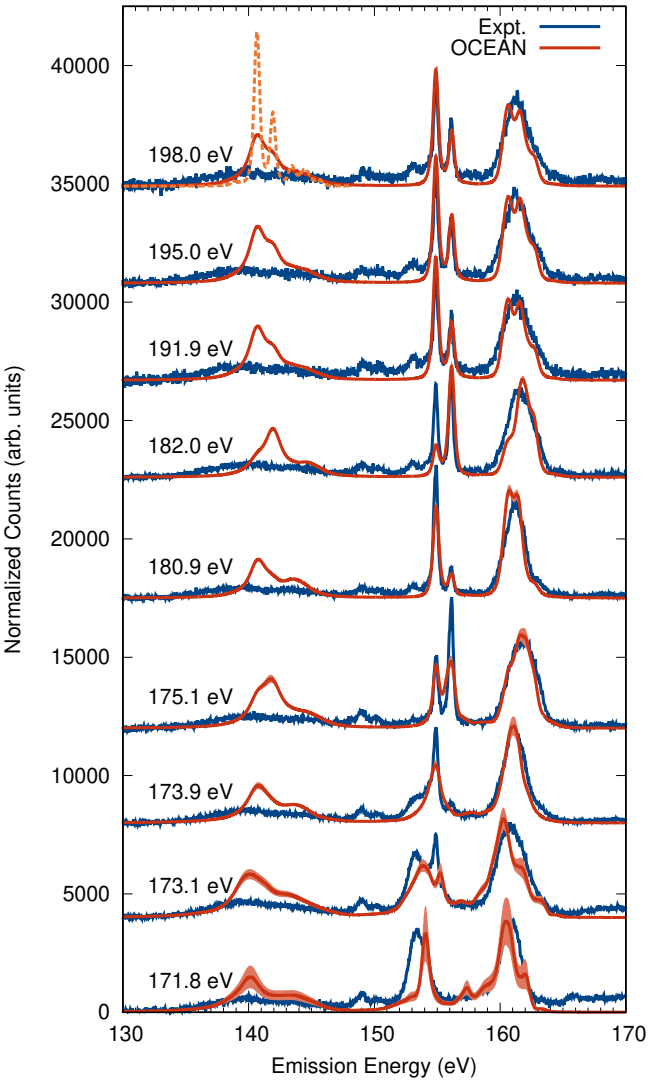

FIG. 4. X-ray emission spectra of Na_2SO_4 (dark, blue) taken at a series of excitation energies above the S $L_{2,3}$-edge with the calculated spectra (light, red), where shaded regions denote the statistical uncertainty from averaging over only 10 snapshots. The orange dashed curve at the highest incident energy shows the theoretical spectrum without the self-energy broadening.

imaginary part of the self-energy. While the broadening observed experimentally has been even greater than that predicted by the self-energy correction, the significant aspect is that it only occurs when the *GW* calculation indicates that $|\mathrm{Im}\Sigma| > 0$. This is only observed for core-hole transitions from bands *where the band energy below the top of the valence band is greater than the band gap for that compound*. The calculated energy of the band gap subtracted from the top of the valence band is shown as a dashed line in Figs. 1 and 2.

The double sharp peaks between 180 eV and 182 eV in the XAS are clearly a single feature in the unoccupied electronic structure split by the S $L_{2,3}$ spin-orbit splitting. Not only are they separated by 1.2 eV, but they have a marked difference in their RIXS spectra. For non-resonant spectra, the emission doublet near 155 eV and 156 eV (Fig 4), arises from the narrow bands around 8 eV below the valence band maximum and shows a clear 2:1 ratio. When the absorption is tuned to 180.9 eV, the higher energy emission peak, arising from the filling of an L_2 hole is suppressed, and the situation reverses at 182.0 eV, though the effect is more pronounced in the calculation than in the measurement. Relatedly, the main edge features between 171 eV and 176 eV are a mix of splitting due to vibrational distortion of the SO_4^{2-} tetrahedra and the spin-orbit splitting, as evidenced by the mix of strengths of this emission doublet, though near the edge they are red-shifted as discussed previously.

Lastly, the observed broadening of the lower valence band emission features, around 140 eV, is clearly much larger than calculated. This could be due to the inaccuracy of using just the lowest-order G^0W^0 approximation to describe the lifetime broadening. It is likely also due in part to the role that these orbitals play in SO_4^{-2}. The creation of a hole in these deep bonding orbitals is likely to destabilize the ion, causing a rapid response of the constituent ions such as the ejection of an oxygen atom. Even if the sulfate is reformed with no permanent radiation damage, the short-term, large distortion of the nuclear positions would cause additional broadening associated with these orbitals that is outside of what our calculations can capture.

V. CONCLUSIONS

As in our previous observations of RIXS at the N K-edge of nitrates, the RIXS at the S $L_{2,3}$-edge demonstrate an unexpected large broadening when a core hole is filled from the lowest valence bands. The emission should be visible as extremely narrow lines, owing to the low dispersion evident in the DFT calculations of these bands. However, a large imaginary self-energy is predicted for only the very lowest bands, when many-body theory is taken into account in the *GW* approximation. The discrepancy is explained by considering quasiparticles that can only be created by holes in the lowest energy valence bands, which are otherwise energetically blocked by the band gap. We expect that this is a general phenomenon that should be observed in the RIXS of other insulating compounds.

Additionally, the rapid change with excitation energy in the x-ray emission spectra in the immediate vicinity of the S $L_{2,3}$-edge due to the screening by the exciton is well accounted for in the Bethe-Salpeter equation.

VI. ACKNOWLEDGEMENTS

The authors would like to thank Jan Weser for assistance in setting up the monochromator gas calibration. Certain software packages are identified in this paper to foster understanding. Such identification does not imply recommendation or endorsement by the National Institute of Standards and Technology, nor does it imply that these are necessarily the best available for the purpose.

[1] F. D. Vila, T. Jach, W. T. Elam, J. J. Rehr, and J. D. Denlinger, J. Phys. Chem. A **115**, 3243 (2011).
[2] J. Vinson, T. Jach, W. T. Elam, and J. D. Denlinger, Phys. Rev. B **90**, 205207 (2014), URL `http://link.aps.org/doi/10.1103/PhysRevB.90.205207`.
[3] J. Vinson, T. Jach, M. Müller, R. Unterumsberger, and B. Beckhoff, Phys. Rev. B **94**, 035163 (2016), URL `http://link.aps.org/doi/10.1103/PhysRevB.94.035163`.
[4] J. Vinson, T. Jach, M. Müller, R. Unterumsberger, and B. Beckhoff, Phys. Rev. B **100**, 085143 (2019).
[5] F. Aryasetiawan and O. Gunnarsson, Rep. Prog. Phys. **61**, 237 (1998).
[6] E. V. Rasmussen, J.-E. Jorgensen, and B. Lundtoft, J. Appl. Cryst. **29**, 42 (1996).
[7] J. Vinson, J. J. Rehr, J. J. Kas, and E. L. Shirley, Phys. Rev. B **83**, 115106 (2011), URL `http://link.aps.org/doi/10.1103/PhysRevB.83.115106`.
[8] J. Vinson, Phys. Chem. Chem. Phys. **24**, 12787 (2022), URL `http://dx.doi.org/10.1039/D2CP01030E`.
`www.ocean-code.com`, *v.* 3.1.2.
[9] G. Kresse and J. Hafner, Phys. Rev. B **47**, 558 (1993).
[10] J. Furthmüller and G. Kresse, Comput. Mater. Sci. **6**, 15 (1996).
[11] G. Kresse and J. Furthmüller, Phys. Rev. B **54**, 11169 (1996).
[12] P. E. Blöchl, Phys. Rev. B **50**, 17953 (1994).
[13] H. J. Monkhorst and J. D. Pack, Physical Review B **13**, 5188 (1976).
[14] J. P. Perdew, K. Burke, and M. Ernzerhof, Phys. Rev. Lett. **77**, 3865 (1996), URL `https://link.aps.org/doi/10.1103/PhysRevLett.77.3865`.
[15] S. Grimme, J. Antony, S. Ehrlich, and H. Krieg, J. Chem. Phys. **132**, 154104 (2010).

[16] X. Gonze, B. Amadon, G. Antonius, F. Arnardi, L. Baguet, J.-M. Beuken, J. Bieder, F. Bottin, J. Bouchet, E. Bousquet, et al., Comput. Phys. Commun. **248**, 107042 (2020), URL https://doi.org/10.1016/j.cpc.2019.107042.

[17] X. Gonze, F. Jollet, F. A. Araujo, D. Adams, B. Amadon, T. Applencourt, C. Audouze, J.-M. Beuken, J. Bieder, A. Bokhanchuk, et al., Comput. Phys. Comm. **205**, 106 (2016), ISSN 0010-4655, URL http://www.sciencedirect.com/science/article/pii/S0010465516300923.
www.abinit.org *v.* 10.0.7.

[18] M. J. van Setten, M. Giantomassi, E. Bousquet, M. J. Verstraete, D. R. Hamann, X. Gonze, and G.-M. Rignanese, Comput. Phys. Commun. **226**, 39 (2018), URL https://www.sciencedirect.com/science/article/pii/S0010465518300250.
http://www.pseudo-dojo.org Scalar-relativstic *v.* 0.4.

[19] D. R. Hamann, Phys. Rev. B **88**, 085117 (2013), URL https://link.aps.org/doi/10.1103/PhysRevB.88.085117.
The open-source code ONCVPSP is available at http://www.mat-simresearch.com *v.* 3.3.1.

[20] A. A. Mostofi, J. R. Yates, Y.-S. Lee, I. Souza, D. Vanderbilt, and N. Marzari, Comput. Phys. Comm. **178**, 685 (2008), ISSN 0010-4655, URL http://www.sciencedirect.com/science/article/pii/S0010465507004936.

[21] J. Campbell and T. Papp, Atomic Data and Nuclear Data Tables **77**, 1 (2001), ISSN 0092-640X, URL https://www.sciencedirect.com/science/article/pii/S0092640X00908489.

[22] L. Weinhardt, D. Hauschild, R. Steininger, N. Jiang, M. Blum, W. Yang, and C. Heske, Analytical Chemistry **93**, 8300 (2021), https://doi.org/10.1021/acs.analchem.1c01187, URL https://doi.org/10.1021/acs.analchem.1c01187.

[23] P. Giannozzi, O. Andreussi, T. Brumme, O. Bunau, M. B. Nardelli, M. Calandra, R. Car, C. Cavazzoni, D. Ceresoli, M. Cococcioni, et al., J. Phys.: Condens. Matter **29**, 465901 (2017), URL http://stacks.iop.org/0953-8984/29/i=46/a=465901.

[24] P. Giannozzi et al., J. Phys. Condens. Matter **21**, 395502 (2009).
www.quantum-espresso.org *v.* 7.3.

[25] F. Scholze, B. Beckhoff, G. Brandt, R. Fliegauf, R. Klein, B. Meyer, D. Rost, D. Schmitz, M. Veldkamp, J. Weser, et al., Proc. SPIE **4146**, 72 (2000).

[26] E. Hudson, D. Shirley, M. Domke, G. Remmers, A. Puschmann, T. Mandel, C. Xue, and G. Kaindl, Phys. Rev. A **47**, 361 (1993).

[27] M. Müller, B. Beckhoff, R. Fliegauf, and B. Kanngießer, Phys. Rev. A **79**, 032503 (2009).

[28] M. C. Hettrick and J. H. Underwood, Appl. Opt. **25**, 4228 (1986).